Chapter 3

Practical Limits to the Detection, Localization, and Characterization of Optical Inhomogeneities with Diffuse Photon Density Waves

In the previous chapter I demonstrated various physical properties of diffuse photon density waves (DPDW's), and showed that DPDW's are perturbed by the presence of optical inhomogeneities and that by measuring the perturbation of a DPDW it is possible to detect, localize, and characterize the inhomogeneities. It is desirable to establish fundamental limits for the detection, localization, and characterization of optical inhomogeneities in order to assess the degree with which diffusing photons can be effectively used to provide physiological information about tissues. An understanding of these limiting factors will lead to the optimization of medical optical imaging prototypes.

Since measurements are made in the near-field (i.e. within one DPDW wavelength of the source) the usual diffraction criteria are inadequate for resolution determinations. In the near-field, resolution is intimately related to the signal-to-noise ratio of the measurement. The resolving power of DPDW's has been studied within this context by comparing the amplitude of the spatial frequencies with the noise level [89]. Additionally, the resolving power of pulse-time measurements has been examined using temporal point spread functions [90, 91, 92, 93, 94]. No analysis, however, has been made that focuses on limitations for the detection, localization, and characterization of optical inhomogeneities with DPDW's.

This chapter presents such an analysis. The signals are calculated using the analytic model for the scattering of DPDW's discussed in section 2.5 [29, 30, 31]. Two different noise models are considered: shot-noise and random errors due to positional uncertainty of the source and detector. My analysis indicates that uncertainties in source, detector, and sample position limits detection to millimeter size objects, and full optical characterization to centimeter size objects. I show how small improvements can be made by optimizing the measurement geometry and source modulation frequency. I find that modulation frequencies less than 500 MHz are optimal for detection and characterization. For higher modulation frequencies the noise threshold increases with the modulation frequency more than the relevant signal. In addition, I show that spectral measurements (i.e. using DPDW information at several source modulation frequencies) enhance the characterization of scattering objects but not absorbing objects. Schemes for optimizing measurement protocols for clinically relevant systems are discussed.

3.1 The Models

In order to determine the limits for detection and characterization of localized heterogeneities, I utilize exact models. A spherical inhomogeneity embedded in an otherwise homogeneous turbid medium is used as the standard system (see fig. 3.1) for assessing the limits. The turbid medium is an infinite slab of finite thickness. Measurements are made in transmission mode at a single photon wavelength. For an ideal experimental system, the signal-to-noise ratio is shot-noise limited and thus scales with the square-root of the number of photons detected. However, there are other sources of random error that exceed shot-noise, such as the positional uncertainty of the source and detector relative to the sample. I consider these effects in the following sections.

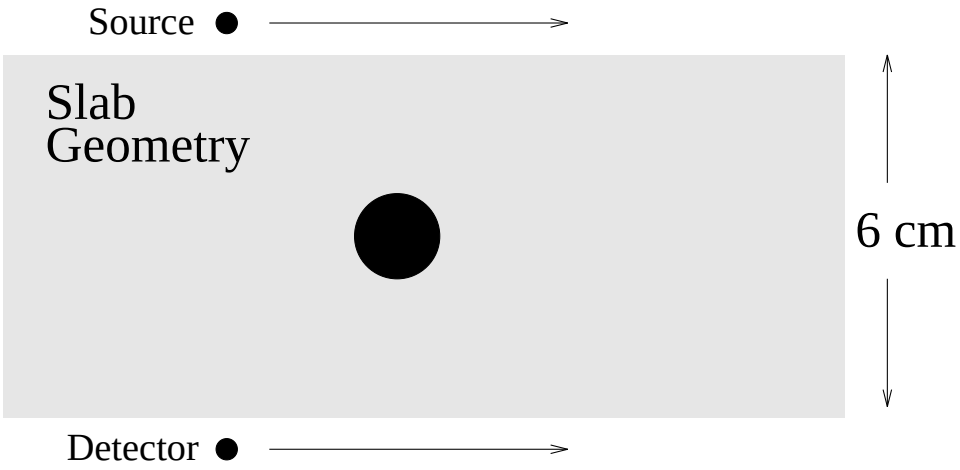

Figure 3.1: Diffuse Photon Density Waves are generated by injecting light from a sinusoidally modulated source into a turbid medium. The 3 mW, 780 nm source is modulated at 200 MHz. The turbid medium is 6.0 cm thick with a reduced scattering coefficient, μ_s', of 10.0 cm^{-1} and μ_a = 0.05 cm^{-1}. A spherical object is embedded in the middle of the slab. Light is collected and delivered to a photo-multiplier tube via an optical fiber with an aperture of 0.4 cm. For the simulations, the source and detector are scanned together along the boundary, or the source is held fixed close to the object and the detector is scanned. Two different objects are studied; an absorbing object with $\mu_{s,in}'$ = 10.0 cm^{-1} and $\mu_{a,in}$ = 0.15 cm^{-1} and a scattering object with $\mu_{s,in}'$ = 15.0 cm^{-1} and $\mu_{a,in}$ = 0.05 cm^{-1}. Other parameters are considered as indicated in the text.

3.1.1 Analytic Solution for the Signal

To calculate the signal resulting from the inhomogeneity in fig. 3.1, I use the analytic solution for the scattering of the DPDW's discussed in chapter 2.5 [29, 30, 31]. This method is exact provided that the diffusion approximation to the transport equation is valid. The analytic solution reveals that the measured DPDW outside the object is simply a superposition of the incident diffuse photon density wave plus the diffusive wave scattered from the object, i.e.

$$\Phi(\mathbf{r_s}, \mathbf{r_d}) = vS_{AC}\frac{\exp(ik_{out}|\mathbf{r_s} - \mathbf{r_d}|)}{4\pi D_{out}|\mathbf{r_s} - \mathbf{r_d}|} + \sum_{l=0}^{\infty} A_l h_l^{(1)}(k_{out} r_d) Y_l^0(\hat{\Omega}_d) \ . \tag{3.1}$$

Here, the position of the source (detector) is denoted by $\mathbf{r_s}$ ($\mathbf{r_d}$) and the object is centered at the origin. S is the modulation amplitude of the source in photons per second. k_{out} is the wavenumber of the DPDW outside the object and is given by $k_{out}^2 = \frac{-v\mu_{a,out}+i\omega}{D_{out}}$, where v is the speed of light in the medium, $D_{out} = v/(3\mu'_{s,out})$ is the photon diffusion coefficient, $\mu'_{s,out}$ is the reduced scattering coefficient and $\mu_{a,out}$ is the absorption coefficient of the background medium, and $\omega = 2\pi f$ is the angular frequency of the DPDW (f denotes the modulation frequency). For the scattered wave, $h_l^{(1)}(x)$ are Hankel functions of the first kind and $Y_l^0(\hat{\Omega})$ are the spherical harmonics with the azimuthal index equal to zero since the source is taken to be on the z-axis and the object is at the origin (i.e. the system has azimuthal symmetry). The scattered wave is written as a series of partial-waves or multipole moments where the amplitude of each partial wave is given by the scattering amplitude A_l (see eq. (2.35)).

In general, the scattering amplitudes, A_l, depend on the diameter of the spherical object, the optical properties of the object and the background medium, and the source modulation frequency. Detection and characterization of the optical inhomogeneities depend on the magnitude of the different partial-waves or moments of the scattered DPDW. The most important moments of the scattered wave are the monopole ($\Phi_{sc}^{l=0}$), dipole ($\Phi_{sc}^{l=1}$), and quadrupole ($\Phi_{sc}^{l=2}$). To leading order in $k_{out}a$ and $k_{in}a$, assuming $|k_{out}a| \ll 1$ and $|k_{in}a| \ll 1$ (where k_{in} is the DPDW wavenumber inside the spherical

object and a is the radius of the object) these moments are

$$\Phi_{sc}^{l=0} = vS_{AC}\frac{\exp(ikr_s)}{4\pi D_{out}r_s}\frac{\exp(ikr_d)}{4\pi r_d}\left[\frac{4\pi a^3}{3}\right]\left[\frac{-v\delta\mu_a}{D_{out}}\right] \quad , \tag{3.2}$$

$$\Phi_{sc}^{l=1} = vS_{AC}\frac{\exp(ikr_s)}{4\pi D_{out}r_s}\frac{\exp(ikr_d)}{4\pi r_d}\left[ik-\frac{1}{r_s}\right]\left[ik-\frac{1}{r_d}\right]\left[\frac{4\pi a^3}{3}\right]\left[\frac{-3\cos\theta\delta\mu_s'}{3\mu_{s,out}'+2\delta\mu_s'}\right] \quad , \tag{3.3}$$

$$\begin{aligned}\Phi_{sc}^{l=2} \quad = \quad & vS_{AC}\frac{\exp(ikr_s)}{4\pi D_{out}r_s}\frac{\exp(ikr_d)}{4\pi r_d}\left[k^2+\frac{3ik}{r_s}-\frac{3}{r_s^2}\right]\left[k^2+\frac{3ik}{r_d}-\frac{3}{r_d^2}\right]\left[3\cos^2\theta-1\right] \\ & \left[\frac{4\pi a^5}{45}\right]\left[\frac{\delta\mu_s'}{5\mu_{s,out}'+3\delta\mu_s'}\right] \quad . \end{aligned} \tag{3.4}$$

Here, $\delta\mu_a = \mu_{a,in} - \mu_{a,out}$ is the difference in the absorption coefficient of the object and background, $\delta\mu_s' = \mu_{s,in}' - \mu_{s,out}'$ is the difference in the reduced scattering coefficient, $k = k_{out}$, and θ is the angle between the z-axis and the line joining the detector to the object center. To leading order $\Phi_{sc}^{l=0}$ depends only on $\delta\mu_a$ and $\Phi_{sc}^{l=1}$ and $\Phi_{sc}^{l=2}$ depend only on $\delta\mu_s'$. We have to look at higher order terms for the Φ_{sc}^{l} to see dependences on the other optical properties.

For an object that has the same scattering properties as the background, but different absorption properties, the signal is derived to leading order from the monopole term and scales as $a^3\delta\mu_a$. Thus, to leading order one can only reconstruct the product $a^3\delta\mu_a$ and cannot simultaneously determine the diameter and absorption coefficient of the object. When the monopole is the only detectable moment, a small, highly absorbing object cannot be distinguished from a larger, less absorbing object. The dipole and quadrupole moments have a different functional dependence on a and $\delta\mu_a$ and thus the object can be characterized, in principle, when both the monopole and either the dipole or the quadrupole moments are detectable.

The results are similar for an object with a pure scattering change. In that case, the dominate term is the dipole moment which depends on the product of a^3 and $\delta\mu_s'$. The size and scattering coefficient of a scattering object, therefore, cannot be simultaneously characterized unless the dipole and quadrupole moments are detectable. Generally, the detectability of the different moments of the scattered DPDW depends on the characteristics of the object and the noise in the measurements.

3.1.2 Noise Models

For an ideal experimental system the uncertainty in the measured amplitude and phase of the DPDW is given by shot-noise. Shot-noise is defined as the square-root of the number of photons detected. In practice, however, the uncertainty in the DPDW amplitude and phase is not dominated by shot-noise but is also affected by uncertainty in the position of the source and detector relative to one another and relative to the sample (see fig. 3.2). There are two different types of positional uncertainty. They are: 1) random errors associated with the incorrect positioning of the source and detector such that the actual distance of the source and detector with respect to each other and with respect to a reference point exhibits a normal distribution about the expected value, and 2) random errors from small motions of the sample, e.g. due to breathing and the heart pulse. An important difference between these two sources of positional errors is that the second type can be reduced by integration of the signal over longer times while the first type, in principle, can only reduced by repeated trials wherein the source and detector are actually repositioned. In our laboratory we have found (in an infinite homogeneous medium) that the positional uncertainty is the leading contributor to the uncertainty in the amplitude and phase of the DPDW. For a given source-detector pair, with a positional uncertainty σ_r, the fractional uncertainty in the amplitude, $\frac{\sigma_{AC}}{|\Phi(\mathbf{r_s},\mathbf{r_d})|}$, in an infinite medium is given by

$$\begin{aligned}\frac{\sigma_{AC}}{|\Phi(\mathbf{r_s},\mathbf{r_d})|} &= \left[\mathrm{Im}(k)+\frac{1}{|\mathbf{r_s}-\mathbf{r_d}|}\right]\sigma_r \\ &= \left[\sqrt{\frac{3}{2}}\sqrt{\mu_a\mu_s'}\left(\sqrt{1+(\frac{\omega}{v\mu_a})^2}-1\right)^{\frac{1}{2}}+\frac{1}{|\mathbf{r_s}-\mathbf{r_d}|}\right]\sigma_r\ , \qquad (3.5)\end{aligned}$$

and the uncertainty in the phase in radians, σ_θ, in an infinite medium is given by

$$\begin{aligned}\sigma_\theta &= \mathrm{Re}(k)\sigma_r \\ &= \sqrt{\frac{3}{2}}\sqrt{\mu_a\mu_s'}\left(\sqrt{1+\left(\frac{\omega}{v\mu_a}\right)^2}+1\right)^{\frac{1}{2}}\sigma_r\ . \qquad (3.6)\end{aligned}$$

$|\Phi(\mathbf{r_s}, \mathbf{r_d})|$ is the amplitude of the detected DPDW, Im(k) is the imaginary part of the DPDW wavenumber, and Re(k) is the real part of the DPDW wavenumber. The noise in the amplitude decreases with increasing attenuation length of the DPDW. The noise in the phase decreases with increasing wavelength of the DPDW. Thus, a variation of system parameters which result in a decrease in the DPDW attenuation length and wavelength will increase the noise due to source-detector positional uncertainties. We have verified this relation with the equipment in our lab which has a positional uncertainty of 0.1 mm. To do so, we repeatably measured the amplitude and phase of the DPDW in an infinite medium at various source-detector separations and compared the measured uncertainties with those calculated using eq. (3.5) and eq. (3.6). This process was then repeated for systems with different optical properties and in all cases good agreement was observed. Eq. (3.5) and eq. (3.6) are a reasonable approximation of the amplitude and phase uncertainties that arise due to positional uncertainties in semi-infinite and slab geometries. For semi-infinite and slab geometries I do not write down the exact equation for the uncertainties. Calculations of the change in amplitude and phase for small displacements of the source and detector for such geometries show that the uncertainties are well approximated by eq. (3.5) and eq. (3.6).

An estimation of the magnitude of shot-noise and noise from positional errors indicates the significance of positional uncertainties. I estimate a clinically relevant shot-noise using a 3 mW light source with 100% modulation, a detector with a collection area of 0.1 cm^2, a quantum efficiency of 1%, and the experimental system depicted in fig. 3.1. With these parameters, shot-noise gives a fractional error of 9x10^{-4} in the wave amplitude for a one second integration time (the phase noise is 9x10^{-4} radians or $\sim$0.05°). For a positional uncertainty of 10 μm in either the source or the detector, the fractional error in the amplitude is 2x10^{-3} and the phase noise is 0.03°. If the uncertainty is in the position of both the source and detector then the noise threshold is multiplied by $\sqrt{2}$. For a typical clinical situation the noise produced from positional uncertainties in the source and detector is comparable to shot-noise.

Achieving a positional certainty of 10 μm in the clinic is a daunting task consid-

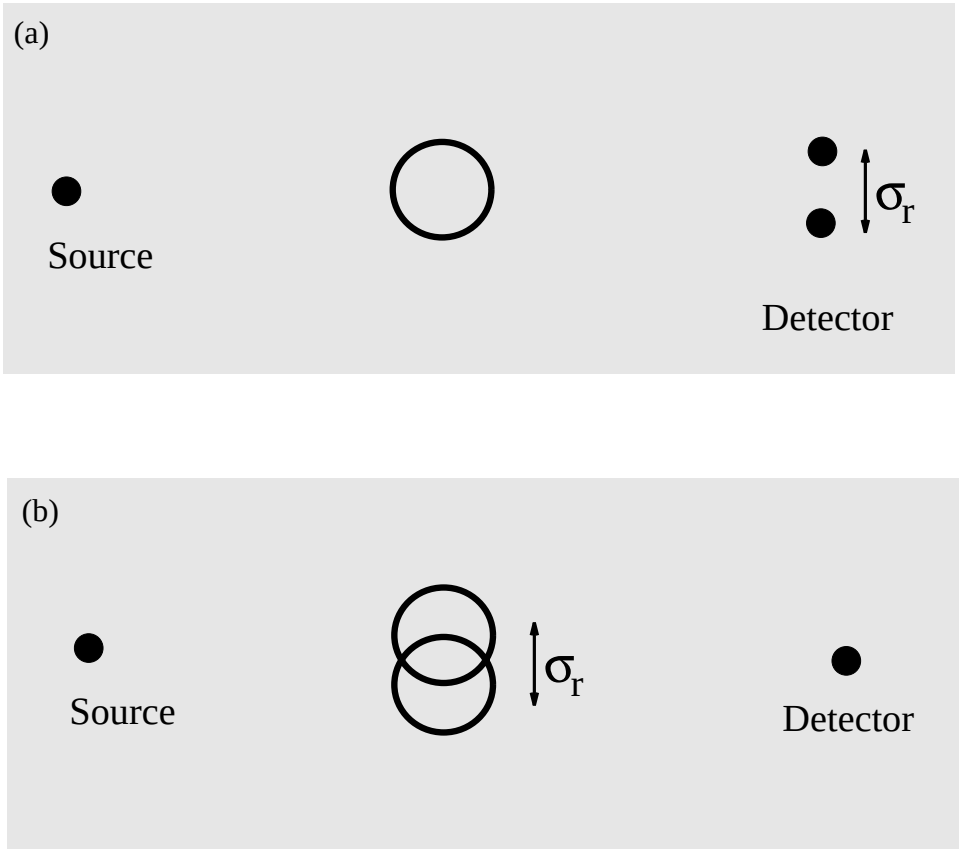

Figure 3.2: Errors from positional uncertainty can arise from an inaccurate positioning of the source and detector relative to each other (as depicted in (a)) and/or relative to the sample under study (as shown in (b)). These errors are random unless no vibrations are present and no realignment of the source and detector are made for multiple measurements. In a clinical environment vibrations will be present due to breathing and the heart beat. In case (a) and (b) σ_r is reduced by making repeated measurements. Positional uncertainties induced by sample vibrations of type (b) are reduced by longer integration times.

ering the motional artifacts arising from the respiration and pulse of the subjects. A more realistic positional uncertainty of 100 μm will result in a 2% uncertainty in the amplitude and 0.3° degree uncertainty in the phase. These results are for a best case scenario and are based on the shot-noise arising under the above described conditions and the additional noise arising from a positional uncertainty of 10 μm. These two types of noise will be reduced by the $\sqrt{N}$ where N is the number of independent measurements averaged to obtain a single value for the amplitude and the phase.

3.2 Description of Simulations

All results in this chapter for the detection and characterization of optical inhomogeneities using DPDW's are based on analytic calculations of the distorted DPDW with appropriate levels of random noise. The sample is an infinite slab, 6 cm thick (~60 random walk steps thick) which is homogeneous except for a spherical heterogeneity centered between the input and output planes of the slab. Measurements are made in transmission mode, i.e. the source is on one side of the slab and the detector is on the other side. Two types of spherical objects are considered: an absorbing object which has the same scattering coefficient as the background, and a scattering object which has the same absorption coefficient as the background.

To study the limits for detection and localization of these objects, the source and detector are scanned together along the surface of the slab. The perturbation to the amplitude and phase of the DPDW by the object can be described, respectively, by the ratio of the amplitudes with and without the object and the difference in the phase with and without the object.

In Section 3.3 the detectability of the object is found by comparing this perturbation with the noise level. If the perturbation is greater than the noise level, the object is deemed detectable. A large portion of parameter space is studied by varying the background optical properties, the object optical properties, and the DPDW modulation frequency. Note that at each detector position the signal is integrated for

1 second and measured once. Shot-noise can be reduced by increasing the integration time while the noise due to positional errors can be reduced by averaging repeated measurements in which the source and detector are physically repositioned. If the positional errors are due to movement of the sample, then the noise is also reduced by increasing the integration time.

The ultimate clinical applications of these probes may depend on our capabilities for object characterization. For example, to specify tumor size and malignancy or brain bleed maturity, it is likely that the size and optical properties of the detectable optical inhomogeneity will need to be characterized. In section 3.4 limits to object characterization are studied by first calculating the perturbed DPDW and then estimating the uncertainty with which the object's size and optical properties can be determined by means of a chi-squared fitting procedure to the analytic solution. The perturbed DPDW is first calculated using the analytic solution and then appropriate noise is added. "Measurements" are made with the source fixed at a position closest to the object at x=0 and z=0, and the detector scanned from x=-2.0 to 2.0 cm in steps of 0.20 cm at z=6.0 cm. A total of 42 independent measurements are obtained (21 amplitude and 21 phase measurements). In all studies the DPDW modulation frequency is 200 MHz. The noise added in these measurements is that given by the shot-noise for a 3 mW source and the noise from random positional uncertainties of 10 μm as described in section 3.1.2. Thus the noise used in the simulations is approximately 0.3% in the amplitude and 0.08° phase.

The fitting procedure is based on minimizing the chi-square difference between the measured DPDW profile and the analytic solution by varying the object's diameter and optical properties. This procedure is a best case scenario since we assume the background optical properties as well as the position and shape of the object. In practice more general imaging methods must be used that do not assume that the shape of the object is known. My results therefore represent the best one can possibly do in terms of characterization for a specific set of measurements. For a given noise level, the uncertainty in the estimated properties is found using the chi-squared method

described by Bevington [95]. In essence, the uncertainty of a fit parameter is found by varying the parameter until the chi-square value increases by one from the value at the global minimum. Theoretically, the uncertainty determined in this way is equivalent to the uncertainty that would be found from multiple experiments.

The chi-square difference function to be minimized is

$$\chi^2(\mu_s', \mu_a, a) = \sum_{i=1}^{N} \frac{\left[|\Phi^i_{\text{exp}}(\mathbf{r_s}^i, \mathbf{r_d}^i)| - |\Phi^i_{\text{anal}}(\mathbf{r_s}^i, \mathbf{r_d}^i, \mu'_{s,in}, \mu_{a,in}, a)|\right]^2}{\sigma^{i2}_{AC}} + \frac{\left[\text{Arg}[\Phi^i_{\text{exp}}(\mathbf{r_s}^i, \mathbf{r_d}^i)] - \text{Arg}[\Phi^i_{\text{anal}}(\mathbf{r_s}^i, \mathbf{r_d}^i, \mu'_{s,in}, \mu_{a,in}, a)]\right]^2}{\sigma^{i2}_{\theta}} . \quad (3.7)$$

Here, the sum is over all measurements, $\mathbf{r_s}^i$ and $\mathbf{r_d}^i$ are the position of the source and detector for the ith measurement, $\Phi^i_{exp}(\mathbf{r_s}^i, \mathbf{r_d}^i)$ is the experimental photon fluence for this pair, and $\Phi^i_{anal}(\mathbf{r_s}^i, \mathbf{r_d}^i, \mu'_{s,in}, \mu_{a,in}, a)$ is the fluence obtained from the analytic solution (eq. (3.1)) using the optical characteristics of the object (i.e. $\mu'_{s,in}$, $\mu_{a,in}$, and a). Recall that $\Phi^i_{exp}(\mathbf{r_s}^i, \mathbf{r_d}^i)$ is obtained by adding random noise to the analytic solution (eq. (3.1)). The vertical bars, $|\Phi|$, indicate the absolute value of the complex number and Arg[Φ] represents the phase of the complex number Φ.

The initial amplitude and phase of the source are known. Uncertainty in the amplitude and phase of the source introduces systematic errors, further complicating the characterization procedure. If such uncertainty is present, then the initial phase and amplitude of the source can also be used as free parameters in the χ^2 fit at the expense of increasing the uncertainty in the other fitting parameters.

3.3 Detection and Localization

Breast tumors and brain bleeds are optical inhomogeneities in the sense that their optical scattering and absorption properties are different than that of the surrounding media. An understanding of the detection limits of these inhomogeneities is important for designing optical screening techniques. An optical inhomogeneity is said to be

detectable if the perturbation to the detected amplitude or phase of the DPDW is larger than the noise threshold.

We can detect absorbing objects as small as 3 mm when the object absorption coefficient is a factor of 3 larger than the background. We can detect scattering objects as small as 4 mm when the object scattering coefficient is a factor of 1.5 larger than the background. The small absorbing objects are detectable because of perturbations to the amplitude of the DPDW, while scattering objects are detectable because of perturbations to the phase of the DPDW. The detectability of objects with different contrast is determined by the $a^3\delta\mu_a$ ($a^3\delta\mu_s'$) dependence of the leading order multipole moment of the DPDW scattered from an absorbing (scattering) object. Generally the detectability of an object is determined by the magnitude of $a^3\delta\mu_a$ or $a^3\delta\mu_s'$. For example, a 3 mm diameter absorber with $\delta\mu_a$=0.10 cm^{-1} is detectable, then a 1 mm object with $\delta\mu_a$=2.7 cm^{-1} is also detectable for the same system. This rule of thumb is discussed further in Section 3.6.

3.3.1 Detection of Absorbing Objects

Fig. 3.3 plots the change in the amplitude and phase of the DPDW due to a spherical absorber with $\mu_{a,in} = 0.15$ cm^{-1} embedded in a system with $\mu_{s,out}' = 10.0$ cm^{-1} and $\mu_{a,out} = 0.05$ cm^{-1}. Details of the system are described in fig. 3.1. Results are plotted for 1 mm, 2 mm, and 3 mm diameter absorbers. Given the previously discussed noise threshold, the absorber can be detected if its diameter is at least 3 mm. Note that the largest change in the signal occurs when the object lies directly between the source and detector. Thus if the object is detectable, its transverse position can be determined. By scanning the source and detector along three orthogonal axes, the central coordinates of a detectable object are easily determined. The certainty in the determined position of the object is in principle set by the accuracy in the position of the source and detector.

Fig. 3.4 presents contour plots of the smallest detectable absorber for a large portion of parameter space. Note that the noise levels depend on the factors that

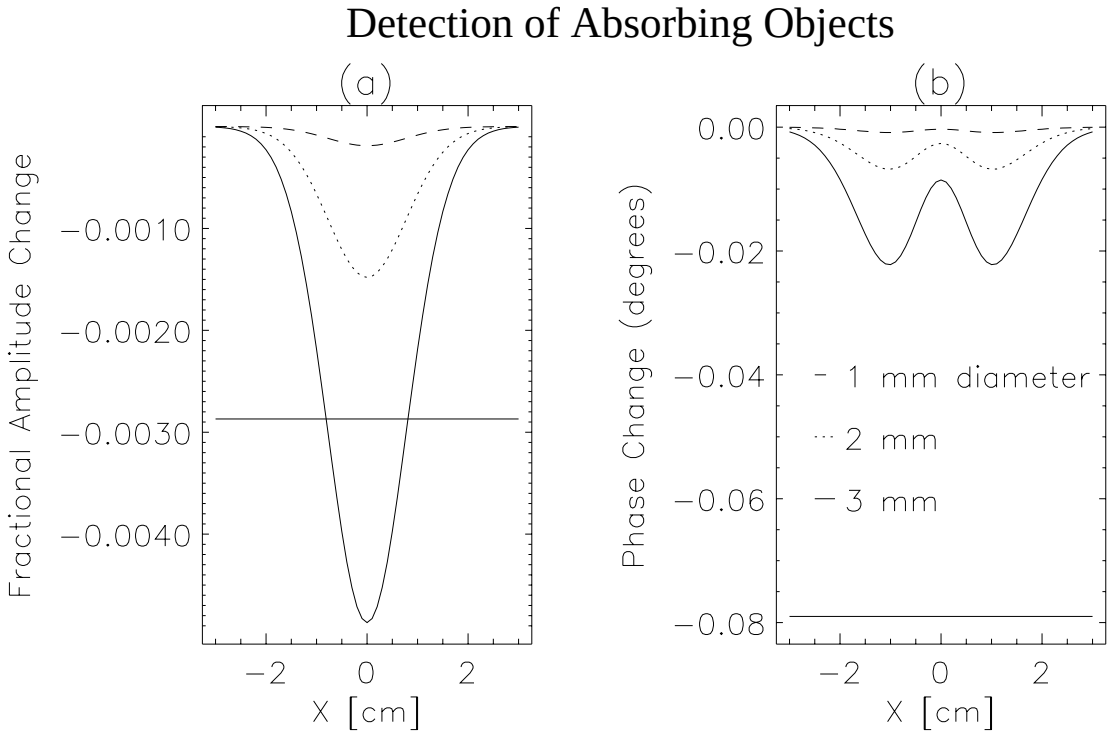

Figure 3.3: The fractional change in the amplitude and change in degrees of the phase due to the presence of the absorbing object is given in (a) and (b) respectively as a function of the lateral position of the source-detector. The system is described in the caption of fig. 3.1. Results are given for 1.0 mm (dashed line), 2.0 mm (dotted line), and 3.0 mm (solid line) diameter absorbers. The noise threshold is given by the solid horizontal line in (a) and (b). Note that the signal does not exceed the noise threshold unless the object's diameter is greater than or equal to 3.0 mm, and then it is only the change in the amplitude and not the phase that is detectable.

are being varied in these graphs and are therefore not fixed at the levels used in fig. 3.3. For example, with a 200 MHz modulation frequency with μ_s'=20.0 cm^{-1} and μ_a=0.05 cm^{-1}, the fractional error in the amplitude is 0.7% and the phase error is 0.3°. With a 200 MHz modulation frequency with μ_s'=10.0 cm^{-1} and μ_a=0.15 cm^{-1}, the fractional error in the amplitude is 1% and the phase error is 0.4°. Recall that with a 200 MHz modulation frequency with μ_s'=10.0 cm^{-1} and μ_a=0.05 cm^{-1}, the fractional error in the amplitude is 0.3% and the phase error is 0.08° so that in fig. 3.4 the noise levels are varying by at least a factor of 5. The noise levels are still determined using a 1 second integration time.

In fig. 3.4a, the contours indicating the diameter of the smallest detectable absorber are drawn as a function of the background reduced scattering coefficient and the object absorption coefficient. The background absorption coefficient was kept fixed and the object reduced scattering coefficient was kept equal to the background reduced scattering coefficient. Clearly, as the object absorption coefficient increases, smaller objects become detectable. The background reduced scattering coefficient has little effect on absorber detectability indicating that the increasing noise, resulting from a larger $\mu_{s,out}'$, is balanced by an increasing signal. The noise increases because of reduced photon transmission through the slab with increased μ_s'. In fig. 3.4b, contours are drawn as functions of the background and object absorption coefficients while keeping the scattering coefficients constant. The detectability of absorbers diminishes as the background absorption coefficient rises because of an increase in shot-noise (due to increased photon absorption) and the decrease in the absorption contrast of the object. In fig. 3.4c, contours are given as a function of source modulation frequency and object absorption coefficient. Surprisingly, increasing the modulation frequency actually decreases the detectability of absorbers. This trend is observed because the noise increases more rapidly than the signal, as discussed further in section 3.5.2 and fig. 3.12.

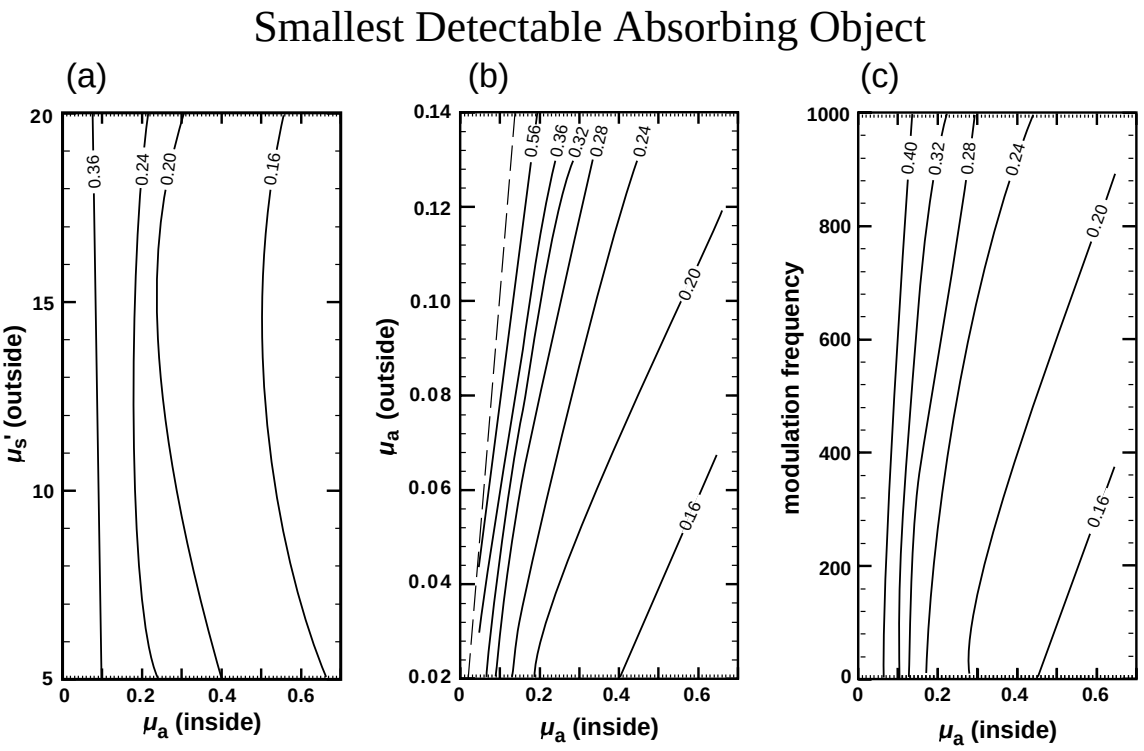

Figure 3.4: The diameter of the smallest detectable absorber is plotted as a function of (a) $\mu'_{s,out}$ and $\mu_{a,in}$, (b) $\mu_{a,out}$ and $\mu_{a,in}$, and (c) source modulation frequency and $\mu_{a,in}$. The contours indicate the diameter of the smallest detectable absorber in units of centimeters. The system and measurements are described in fig. 3.1. In (a), f = 200 MHz, $\mu_{a,out} = 0.05$ cm^{-1}, and $\mu'_{s,in} = \mu'_{s,out}$. In (b), $f = 200$ MHz and $\mu'_{s,out} = \mu'_{s,in} = 10.0$ cm^{-1}. In (c), $\mu'_{s,out} = \mu'_{s,in} = 10.0$ cm^{-1} and $\mu_{a,out} = 0.05$ cm^{-1}. The noise levels are based on a positional uncertainty of 10 μm and a 1 second integration time. The dashed line in (b) indicates where $\mu_{a,out} = \mu_{a,in}$.

3.3.2 Detection of Scattering Objects

Fig. 3.5 graphs the relative change in the signal due to an object with a different reduced scattering coefficient than the background. From fig. 3.5 we see that a 0.4 cm diameter object with a 50% increase in μ_s' relative to the background is detectable. A small scattering object is detectable because the phase shift exceeds the noise threshold while a small absorbing object is detectable because of the relative change in the amplitude. It is because of this distinction that one can ultimately distinguish absorbing and scattering objects. Localization of a scattering object is straightforward since the largest change in the phase occurs when the object is directly between the source and detector.

Contour plots of the smallest detectable scattering object are presented in fig. 3.6. In fig. 3.6a, the smallest detectable object is plotted as a function of background and object reduced scattering coefficient. These results corroborate our expectations that smaller scatterers can be detected when the scattering contrast is increased. In fig. 3.6b, results are plotted as a function of background absorption coefficient and object scattering coefficient. The object absorption coefficient is kept the same as the background. The background absorption coefficient has little effect on the detectability of scattering objects except when the scattering contrast is large. In fig. 3.6c, results are plotted as a function of source modulation frequency and object scattering coefficient. The detectability of the scattering object is relatively unaffected by increasing the modulation frequency, indicating that the noise and signal are increasing at the same rate. In contrast, for the absorbing object, the detectability decreased because the noise increased more than the signal.

3.4 Characterization

After a tumor or brain bleed has been detected and localized, we can then derive information about the inhomogeneity's physical and physiological state by characterizing its size and optical properties. As seen in figs. 3.3 and 3.5 the amplitude and

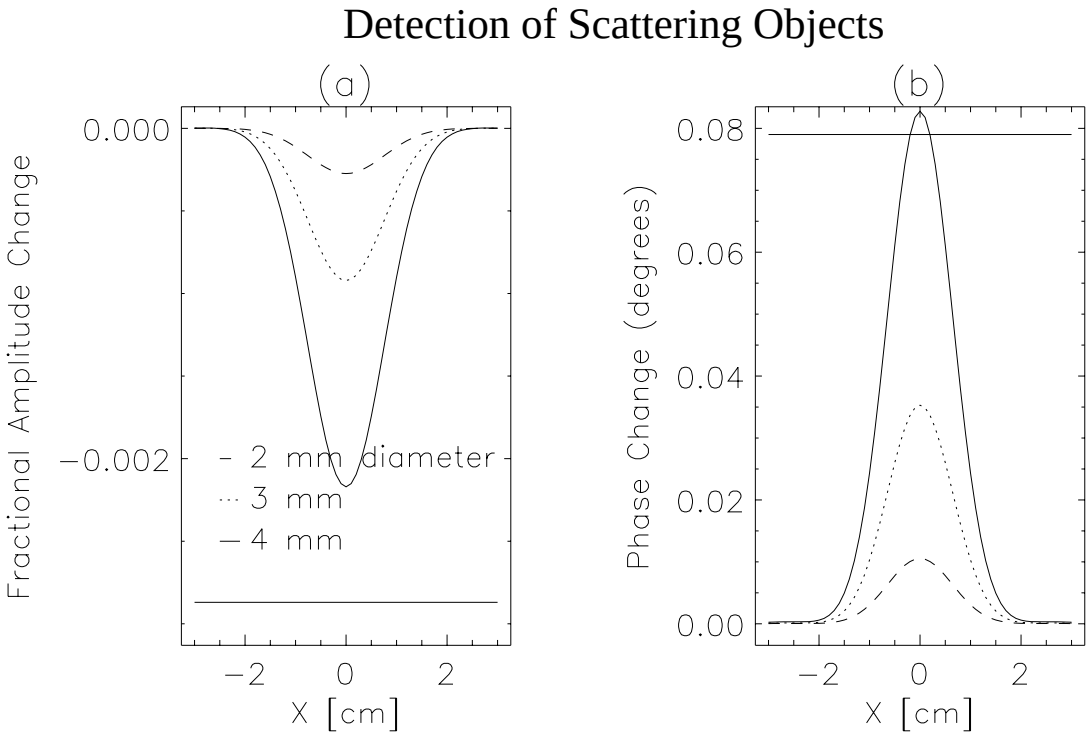

Figure 3.5: The fractional change in the amplitude and change in degrees of the phase due to the scattering object is given in (a) and (b) respectively as a function of the lateral position of the source-detector. The solid line corresponds to a 0.4 cm diameter object, while the dotted and dashed lines correspond to a 0.3 cm and 0.2 cm diameter object respectively. System parameters are described in the caption of fig. 3.1. The noise threshold is given by the solid horizontal line and is 0.3% for the amplitude change and 0.08 degrees phase.

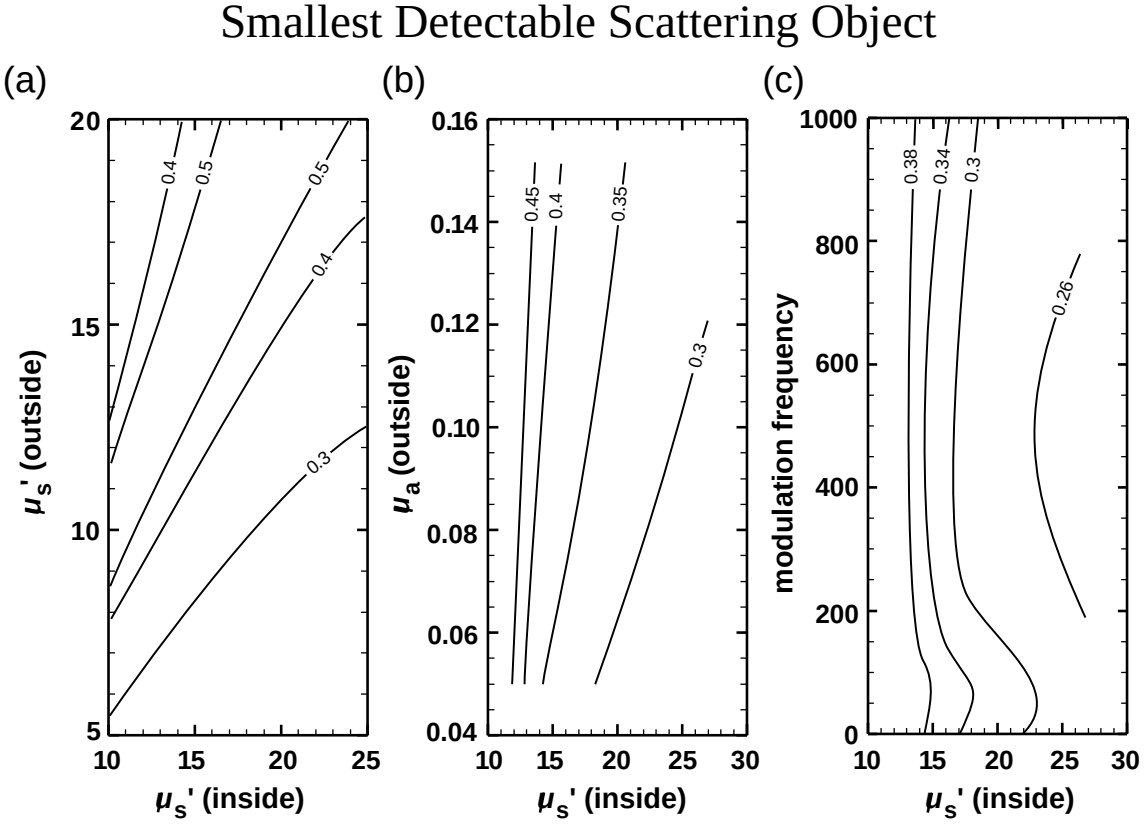

Figure 3.6: The diameter of the smallest detectable scatterer is plotted as a function of (a) $\mu'_{s,out}$ and $\mu'_{s,in}$, (b) $\mu_{a,out}$ and $\mu_{s,in}$, and (c) source modulation frequency and $\mu_{s,in}$. The contours indicate the diameter of the smallest detectable scatterer in units of centimeters. The system and measurements are described in fig. 3.1. In (a), f = 200 MHz and $\mu_{a,out} = \mu_{a,in} = 0.05$ cm^{-1}. In (b), $f = 200$ MHz, $\mu'_{s,out} = 10.0$ cm^{-1}, and $\mu_{a,out} = \mu_{a,in}$. In (c), $\mu'_{s,in} = 10.0$ cm^{-1} and $\mu_{a,out} = \mu_{a,in} = 0.05$ cm^{-1}. The noise levels are based on a positional uncertainty of 10 μm and a 1 second integration time.

phase profile of a distorted DPDW is sensitive to the size of the inhomogeneity as well as the optical properties. Thus, in principle, the characteristics of an inhomogeneity can be determined from the profile of the distorted DPDW. However, in contrast to localization, the size and optical properties cannot be determined directly. We must rely on indirect methods, such as image reconstruction techniques or best fits to analytic solutions for the measured DPDW profile, in order to deduce this information. As described in the experimental section (section 3.2), I use chi-squared fitting techniques to fit for the size and optical properties of the optical inhomogeneity.

3.4.1 Characterization of Absorbing Objects

First I consider simultaneous characterization of the diameter and absorption coefficient of an absorbing object embedded in the center of a 6 cm thick slab (see fig. 3.1). The scattering coefficient of the object is the same as the background, and the detector is scanned from x=-2.0 to 2.0 cm in steps of 0.2 cm while the source is fixed nearest the object at x=0. Fig. 3.7 presents contour plots of the fractional uncertainty of the object's diameter and absorption coefficient. Three different contour plots are given: in fig. 3.7a,b results are given versus object diameter and absorption coefficient ($\mu'_{s,out} = \mu'_{s,in} = 10.0$ cm^{-1}, $\mu_{a,out} = 0.05$ cm^{-1}, and $f = 200$ MHz). In fig. 3.7c,d results are given versus background reduced scattering coefficient and object absorption coefficient ($\mu'_{s,in} = \mu'_{s,out}$, $\mu_{a,out} = 0.05$ cm^{-1}, diameter=1.2 cm, and $f = 200$ MHz). In fig. 3.7e,f results are given versus background absorption coefficient and object absorption coefficient ($\mu'_{s,out} = \mu'_{s,in} = 10.0$ cm^{-1}, diameter=1.2 cm, and $f = 200$ MHz). The system is described in more detail in fig. 3.1. These three contour plots reveal the variation in fractional uncertainty over a large sampling of the parameter space. The magnitude of the uncertainty depends on the total number of measurements that are considered in the χ^2 fit and in general decreases as the square-root of the number of measurements. For the parameter space considered in fig. 3.7, we see that given 21 measurements of the phase and amplitude (for a total of 42 independent measurements), the absorbing object can be accurately characterized when its diameter

exceeds 0.8 cm. Here a 20% uncertainty is considered to be accurate.

The contour plots versus the object's diameter and absorption coefficient (fig. 3.7-a,b) show that the uncertainties diminish rapidly as the diameter increases and slowly as the absorption coefficient is increased. The slower decrease in the uncertainties for larger absorption coefficients results from saturation of the signal. In general the error bar for the diameter is symmetric about the mean value while the error bar for the absorption coefficient of the object is asymmetric. The asymmetry results from the saturation of the signal for larger absorption coefficients. Thus the upper error is always larger than the lower error. The difference is usually within 20%. In all contour plots I plot the average of the lower and upper fractional uncertainties.

From the contour plots versus the background reduced scattering coefficient and the object absorption coefficient (fig. 3.7c,d), we see a similar dependence on the absorption coefficient of the object and that the uncertainties initially decrease and then increase as $\mu'_{s,out}$ increases. The explanation for this is that as $\mu'_{s,out}$ increases, the DPDW wavelength decreases, and as the ratio between the DPDW wavelength and the object diameter gets smaller, the fractional perturbation to the signal increases. Therefore we would expect the uncertainties in the fitting parameters to decrease. However, the noise from positional errors is also increasing because the DPDW wavelength is decreasing. In addition, the shot-noise is increasing because of the reduced transmission through the slab as μ'_s is increased. For the conditons in fig. 3.7c,d, the interplay between the increasing signal and increasing noise is such that the uncertainties first decrease and then increase.

From the contour plots versus the background absorption coefficient and the object absorption coefficient (fig. 3.7e,f), we see that the uncertainties increase as the background absorption coefficient is increased, and they decrease as the object absorption coefficient is increased. There are two factors contributing to the dependence on the background absorption coefficient: first, more light absorption leads to an increase in shot noise, and second, the decrease in the absorption contrast of the object results in a smaller perturbation to the DPDW.

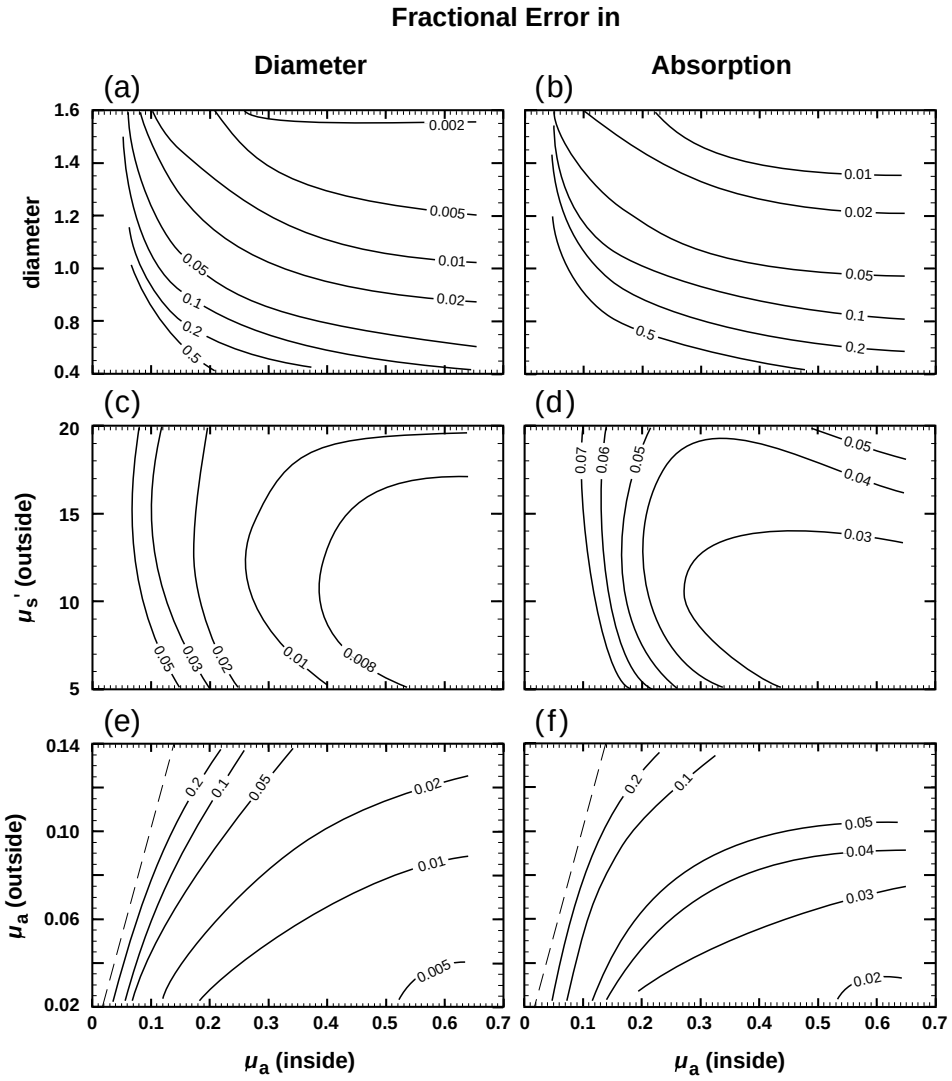

Figure 3.7: The fractional uncertainty in the object diameter (a,c,e) and object absorption coefficient (b,d,f) are plotted in contour plots for a large range of parameter space. The labels on the contours indicate the fractional uncertainty. In (a) and (b) uncertainties are plotted versus the diameter and absorption coefficient of the object. In (c) and (d) the background scattering coefficient and object absorption coefficient are varied. In (e) and (f) the background absorption coefficient and object absorption coefficient are varied. The dashed lines in (e) and (f) indicate where μ_a(outside)=μ_a(inside).

Although a 0.3 cm diameter absorber can be detected and localized, the absorber cannot be characterized accurately unless its diameter is greater than ~0.8 cm. This result was obtained using 21 measurements of amplitude and phase. As discussed in section 3.1.1, this difference between object detection and characterization arises from the functional form of the different moments of the scattered DPDW. Fig. 3.8 plots the contribution of the monopole, dipole, and quadrupole moments of the scattered DPDW to the total signal versus the diameter of the absorbing object. That is, I plot the amplitude and phase of

$$\frac{\Phi_{sc}^{(l)}}{\Phi_{inc}} \ . \tag{3.8}$$

Note that this quantity accounts for the perturbation of each moment to the incident DPDW. If this perturbation is greater than the noise threshold, the given moment of the scattered wave is detectable. The noise threshold is also indicated in the figure.

In order to detect the object it is only necessary for the monopole term to exceed the noise threshold. This occurs when the object's diameter is ≥ 0.3 cm, which agrees with the previous observation in fig. 3.3. The dipole moment does not exceed the noise threshold until the diameter is ≥ 0.8 cm. For absorber diameters $\geq$ 0.8 cm the monopole and dipole moments of the scattered wave are detectable and thus, in principle, the absorber is characterizable. The results in fig. 3.7 indicate that the absorber can be accurately characterized when the diameter exceeds 0.8 cm. Recall that the uncertainty in the object parameters decrease with the square root of the number of measurements and thus accurate characterization of smaller objects is possible by increasing the number of measurements. This may give an experimenter an improvement of 0.3 cm if, for example, 400 measurements are made of the scattered DPDW over the same spatial region as the 40 measurements. This 0.3 cm improvement is estimated from fig. 3.8; if the number of measurements is increased by a factor of ten then the uncertainty will decrease by approximately a factor of three. Thus, from fig. 3.8 we see that the monopole and dipole contributions exceed the noise threshold when the diameter of the absorber exceeds 0.5 cm.

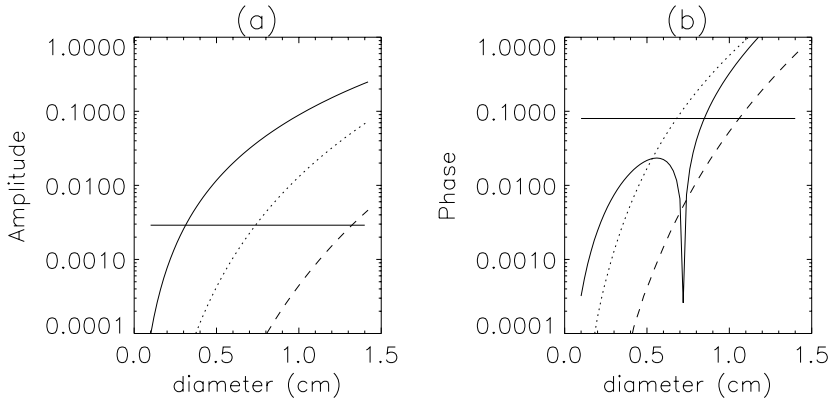

Figure 3.8: The amplitude (a) and phase (b) contribution of the monopole (solid line), dipole (dotted line), and quadrupole (dashed line) moments of the scattered wave to the incident wave is graphed versus the diameter of the absorbing object. The noise threshold is depicted by the horizontal line at $2.9\text{x}10^{-3}$ for the amplitude and $8\text{x}10^{-2}$ for the phase. When the monopole term exceeds the noise threshold at 0.3 cm, then the absorber is detectable. However, the diameter and absorption coefficent of the absorber can not be simultaneously determined until the monopole and dipole terms are detectable. This is the case for diameters greater than 0.8 cm.

3.4.2 Characterization of Scattering Objects

Here I consider the simultaneous characterization of the diameter and scattering coefficient of a scattering object embedded in the center of a 6 cm thick slab (see fig. 3.1). The absorption coefficient of the object is the same as the background, and the detector is scanned from x=-2.0 to 2.0 cm in steps of 0.2 cm while the source is fixed nearest the object at x=0. Fig. 3.9 presents contour plots of the fractional uncertainty of the object's diameter and scattering coefficient. Three different contour plots are given: in fig. 3.9a,b results are given versus object diameter and scattering coefficient ($\mu'_{s,out}$ = 10.0 cm^{-1}, $\mu_{a,out} = \mu_{a,in}$ = 0.05 cm^{-1}, and f = 200 MHz). In fig. 3.9c,d results are given versus background reduced scattering coefficient and object reduced scattering coefficient ($\mu_{a,out} = \mu_{a,in}$ = 0.05 cm^{-1}, diameter=1.2 cm, and f = 200 MHz). In fig. 3.9e,f results are given versus background absorption coefficient and object reduced scattering coefficient ($\mu'_{s,out}$ = 10.0 cm^{-1}, $\mu_{a,out} = \mu_{a,in}$,

diameter=1.2 cm, and f = 200 MHz). The system is described in more detail in fig. 3.1. By plotting these three contour plots we see the variation in the fractional uncertainty over a large sampling of the parameter space. The magnitude of the uncertainty depends on the total number of measurements that are considered in the χ^2 fit and in general decreases as the square-root of the number of measurements. For the parameter space considered in fig. 3.9, we see that, given 21 measurements of the phase and amplitude (for a total of 42 independent measurements), the scattering object can be accurately characterized when its diameter exceeds 0.8 cm. The exact value depends on the scattering coefficient of the object. Again an uncertainty less than 20% is considered accurate.

From the contour plots versus the object's diameter and scattering coefficient (fig. 3.9a,b), we see that the uncertainties diminish rapidly as the diameter increases and slowly as the reduced scattering coefficient is increased. The slower decrease in the uncertainties for larger scattering coefficients results from saturation of the signal and the leading order $a^3\delta\mu_s'$ dependence of the scattered wave. Note that in general the error bar for the diameter is symmetric about the mean value while the error bar for the scattering coefficient of the object is asymmetric. The asymmetry results from the saturation of the signal for larger scattering coefficients and thus the upper error is always larger than the lower error. The difference is usually within 20%. In all contour plots I plot the average of the lower and upper fractional uncertainties.

From the contour plots versus the background reduced scattering coefficient and the object reduced scattering coefficient (fig. 3.9c,d), we first see that the object cannot be characterized when the scattering contrast is smaller than 40%. Interestingly, the fractional uncertainty changes more with a change in the background scattering coefficient than with a change in the object scattering coefficient. One might expect that the uncertainty depends only on the difference in the scattering coefficients in which case changes in the fractional uncertainty would be symmetric with respect to changes in the scattering coefficent of the background and the object. The observed asymmetry results from the noise's dependence on the background reduced scattering

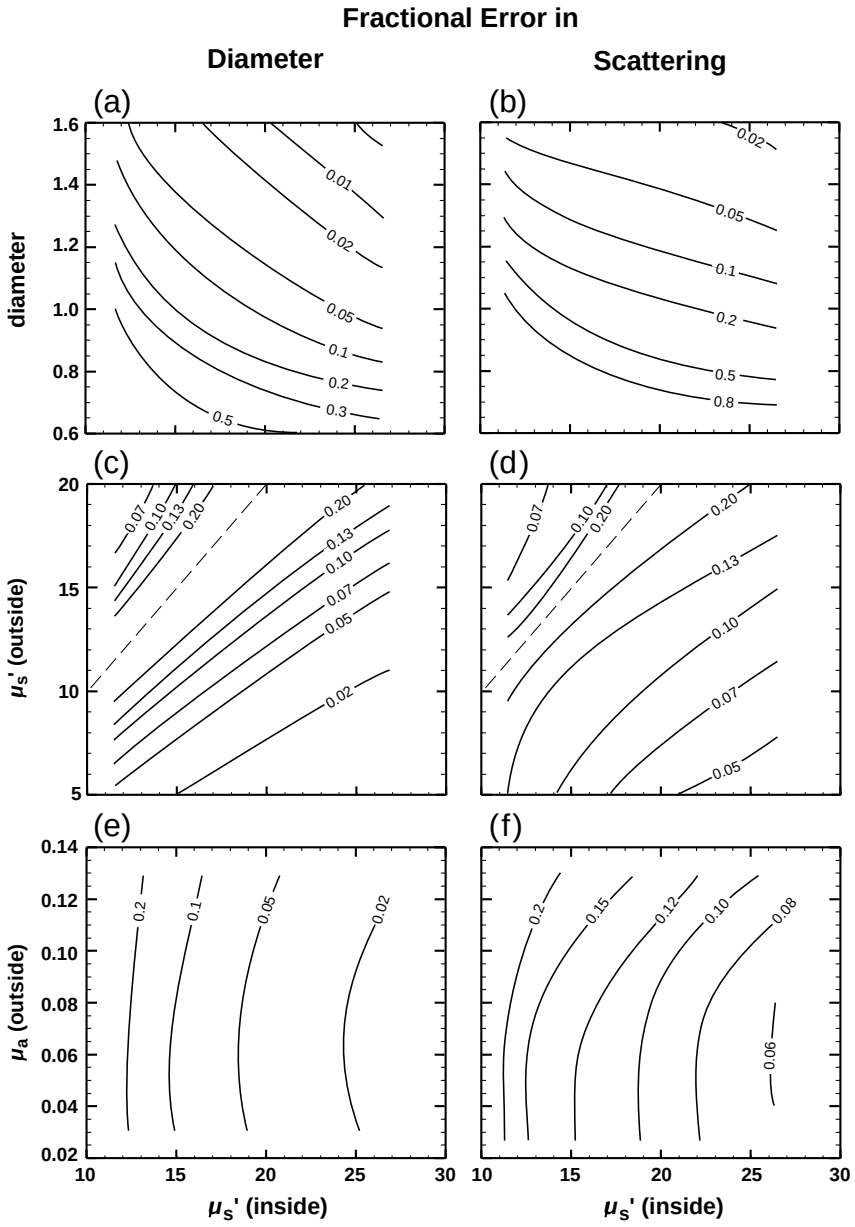

Figure 3.9: The fractional uncertainty in the object diameter (a,c,e) and object scattering coefficient (b,d,f) are plotted in contour plots. The labels on the contours indicate the fractional uncertainty. In (a) and (b) uncertainties are plotted versus the diameter and scattering coefficient of the object. In (c) and (d) the background scattering coefficient and object scattering coefficient are varied. In (e) and (f) the background absorption coefficient and object scattering coefficient are varied. The dashed line in (c) and (d) indicates where μ_s'(outside)=μ_s'(inside).

coefficient. As the background reduced scattering coefficient is increased, the noise also increases because of the reduced transmission of light through the slab (shot-noise) and the decrease in the DPDW wavelength.

From the contour plots versus the background absorption coefficient and the object reduced scattering coefficient (fig. 3.9e,f), we see that the uncertainties increase slightly with an increase in the absorption coefficient and decrease with an increase in the object reduced scattering coefficient. These trends are simply due to the increased shot-noise from increasing the background absorption coefficient and the increased signal from increasing the object reduced scattering coefficient.

Although a 0.4 cm diameter scatterer can be detected and localized, the scatterer cannot be characterized accurately unless its diameter is greater than 0.8 cm. As discussed earlier, this difference between object detection and characterization arises from the functional form of the different moments of the scattered DPDW.

3.5 Optimizing the Experimental Design

Improvements in detecting and characterizing optical inhomogeneities are generally achieved by increasing the signal relative to the noise. The noise threshold can be reduced by making multiple measurements or by integrating the signal longer and reducing shot-noise and positional error due to sample motions. These noise reduction techniques reduce the noise by the square-root of the number of measurements or the square-root of time. The magnitude of the perturbation can be increased by increasing the modulation frequency. Increasing the modulation frequency decreases the DPDW wavelength which in turn results in a larger scattering amplitude, particularly for the higher moments. However, increasing the modulation frequency will increase the shot-noise, as a result of the reduced DPDW amplitude for the same source-detector separation, and increase the uncertainty due to positional errors, as a result of the reduced DPDW wavelength. In the following subsections I investigate the interplay between these various factors.

3.5.1 Optimizing Measurement Geometry

To determine what role the position of the source and detector play in characterizing an object, I repeated the characterization simulation for two different measurement geometries. First the effect of fixing the source closest to the object at $x = 0$ and scanning the detector from x=-3.0 to 3.0 cm in steps of 0.30 cm was examined. The fractional uncertainty in the diameter and absorption coefficient for this set of measurements is graphed in fig. 3.10 along with the previous result obtained from scanning the detector from x=-2.0 to 2.0 cm in steps of 0.20 cm. These results indicate that the characterization accuracy is decreased when the range over which the detector is scanned is increased while keeping the number of measurements constant. The second measurement geometry was chosen to examine the effect of scanning the source and detector together from x=-3.0 to 3.0 cm. For comparison, these results are also plotted in fig. 3.10. The characterization accuracy is decreased further when the source and detector are scanned together. From fig. 3.10 we see that the measurement geometry is optimized for object characterization by keeping the source and detector near the absorbing object. This result applies to scattering objects as well.

These observations are easily understood within the context of the moments analysis. Fig. 3.11 graphs the contribution of each moment to the total signal (eq. (3.8)) versus the transverse position of the detector. Results are plotted for two cases: 1) the source is scanned with the detector and 2) the source is fixed at x=0. The moments are calculated for a 1.0 cm diameter absorber. From fig. 3.11 we see that, overall, the moments make a larger contribution to the scattered wave when the source is fixed near the object. In particular, the perturbation is larger for transverse displacements of the detector from x=0 and therefore it is detectable for a greater number of measurements. By concentrating the measurements where the perturbation is strongest, we are increasing the average signal-to-noise ratio resulting in a more accurate determination of an object's characteristics.

This result suggests that the most accurate characterization will arise from all measurements coming from the source and detector fixed nearest the object. This

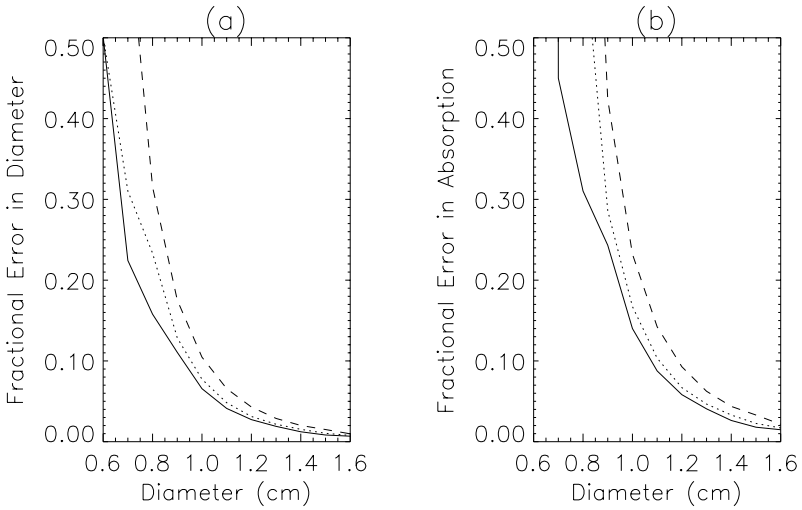

Figure 3.10: The fractional uncertainty for (a) the object diameter and (b) object absorption coefficient are plotted versus the known object diameter for different sets of measurements. The solid line corresponds to the set of measurements presented in fig. 3.7, that is the detector is scanned from x=-2.0 to 2.0 cm while the source is fixed at x=0. The dotted line corresponds to keeping the source fixed at x=0 and scanning the detector from x=-3.0 to 3.0 cm, while for the dashed line the source and detector were scanned together from x=-3.0 to 3.0 cm. In all cases 21 independent measurements of the phase and amplitude were obtained at even intervals over the range of the scan. The system parameters are described in fig. 3.1.

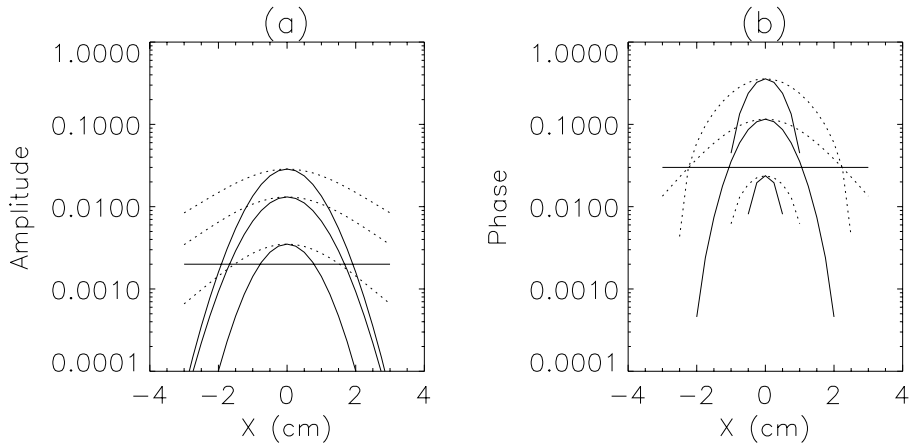

Figure 3.11: The amplitude (a) and phase (b) contribution of the monopole, dipole, and quadrupole moments of the scattered wave to the incident wave is graphed versus the lateral position of the detector. The source was scanned with the detectors for the solid line and fixed at x=0 for the dashed lines. At x=0 the top, middle, and bottom pair of solid and dashed lines correspond respectively to the contributions of the monopole, dipole, and quadrupole moments. The noise threshold is depicted by the horizontal line at $2\text{x}10^{-3}$ for the amplitude and $3\text{x}10^{-2}$ for the phase. When the source is fixed at x=0, i.e. near the object, the signal is larger, permitting an accurate characterization of smaller objects.

is indeed the case when there are only two unknowns, e.g. diameter and absorption coefficient. That is, the amplitude and phase from one source-detector pair provides sufficient information to determine two unknowns. However, if there are more than two unknowns (e.g. initial amplitude and phase of the source, object shape, and/or object position in addition to the diameter and absorption coefficient of the object), then the additional information provided from a spatially distributed set of source-detector pairs is required.

Usually the initial amplitude and phase of the source and the shape of the object will not be known accurately, and therefore measurements from a spatially distributed set of source-detector pairs is optimal. The signal to noise comparison in fig. 3.11 indicates which measurements provide information about the optical inhomogeneity and therefore provides an approach for designing an optimal measurement geometry.

3.5.2 Optimal Modulation Frequency

Comparing signal-to-noise ratios for different DPDW modulation frequencies, we can determine the optimal frequency for detecting and characterizing different objects. Fig. 3.12a,b plots the change in the signal due to each moment relative to the incident wave (eq. 3.8) as a function of modulation frequency for an absorbing object. Although the magnitude of each moment is increasing with frequency, each moment's perturbation of the signal is not necessarily increasing because of interference between the moment and the incident wave. In fact, as is seen in fig. 3.12a,b, at 2200 MHz the quadrupole moment effects no phase shift and at 300 MHz the quadrupole moment effects no amplitude change. These nulls in general do not decrease the ability to characterize an object because a null in either the amplitude or phase is compensated by a large signal in the phase or amplitude respectively. On the other hand, the frequency at which these nulls occur depends on the characteristics of the object and therefore they may be exploited to improve object characterization. A similar idea has been suggested by Yao *et al.* [96].

The shot-noise and positional error as a function of modulation frequency are plot-

ted in fig. 3.12c and d. They exhibit an increase with modulation frequency as expected. For the model system, the shot-noise exceeds the positional noise at frequencies larger than 800 MHz. The crossover point for the amplitude noise occurs because the amplitude of the DPDW is decreasing exponentially as approximately the square-root of the modulation frequency. Thus the fractional error due to shot-noise is increasing exponentially. On the other hand, the fractional error due to positional uncertainty is increasing approximately with the square-root of the modulation frequency. Because of the rapid increase in noise with modulation frequency, measurements at high modulation frequencies are undesirable. Likewise, measurements at low modulation frequencies are undesirable because of the small perturbations.

To determine the optimal frequency for detection and characterization, I calculate the signal-to-noise ratio for the monopole, dipole, and quadrupole moments. These results are plotted in fig. 3.12e and f. The best signal to noise is obtained around 0 MHz. Although the signal-to-noise ratio is smaller at higher modulation frequencies, it is possible to accurately characterize a 1.0 cm diameter absorber at 2.0 GHz, because the monopole and dipole perturbations still exceeds the noise threshold.

Similar results were also obtained for the scattering objects (see fig. 3.13). The main difference is that the best signal-to-noise ratio for scattering objects is obtained around 500 MHz.

Modulation frequencies between 0 and 500 MHz are appropriate when considering the characterization of single objects embedded in otherwise homogeneous systems. If multiple objects are present and resolution becomes an issue, then measurements at higher modulation frequencies are desirable. By resolution I mean the ability to distinguish signals that originate from different sources, e.g. the waves scattered from two distinct objects. Resolution improves with higher modulation frequencies because the DPDW wavelength decreases and we gain sensitivity to smaller length scales. The analytic techniques presented here permit us to determine the maximum modulation frequencies that provide useful information, but they do not provide a simple framework for analyzing the resolving power of DPDW's. The reader is referred

to Pattanayak [89] for a discussion on the resolving power of DPDW's.

3.5.3 Utilizing Spectral Information

It has been suggested that measurements of the amplitude and phase of diffuse photon density waves at several modulation frequencies may be used to enhance sensitivity to the optical properties of a turbid medium [3]. I have investigated this possibility by comparing fractional uncertainties obtained with three different source-detector configurations. The three configurations are: 1) modulation frequency held constant at 200 MHz, 2) modulation frequency scanned from 0 to 1000 MHz in steps of 200 MHz, and 3) modulation frequency scanned from 0 to 1000 MHz in steps of 100 MHz. In each of the three cases, the source was held fixed closest to the object and the detector was scanned from x=-2.0 to 2.0 cm in steps of 0.2 cm. Also, for each case the total number of independent measurements was kept constant at 210 measurements of amplitude and phase (i.e. at each position 10 measurements were made of amplitude and phase). In this way, any observed improvement in the characterization of the object can be attributed to spectral measurements rather than an overall increase in the number of measurements. In case (1) this required making 10 measurements at 200 MHz at each spatial position, while in case (2) 2 measurements where made at each frequency and each spatial position.

Fig. 3.14a,b plots the fractional uncertainty in the diameter and absorption coefficient of an absorbing object versus the diameter of the object for the three different source-detector configurations. No improvement is observed in the fractional uncertainty of the diameter or the absorption coefficient. On the other hand, for a scattering object a decrease in the fractional uncertainty of μ_s' is observed when measurements are made over a range of modulation frequencies (see fig. 3.14c,d). Spectral measurements thus enhance the characterization of scattering objects as well as providing a means of distinguishing scattering from absorbing objects.

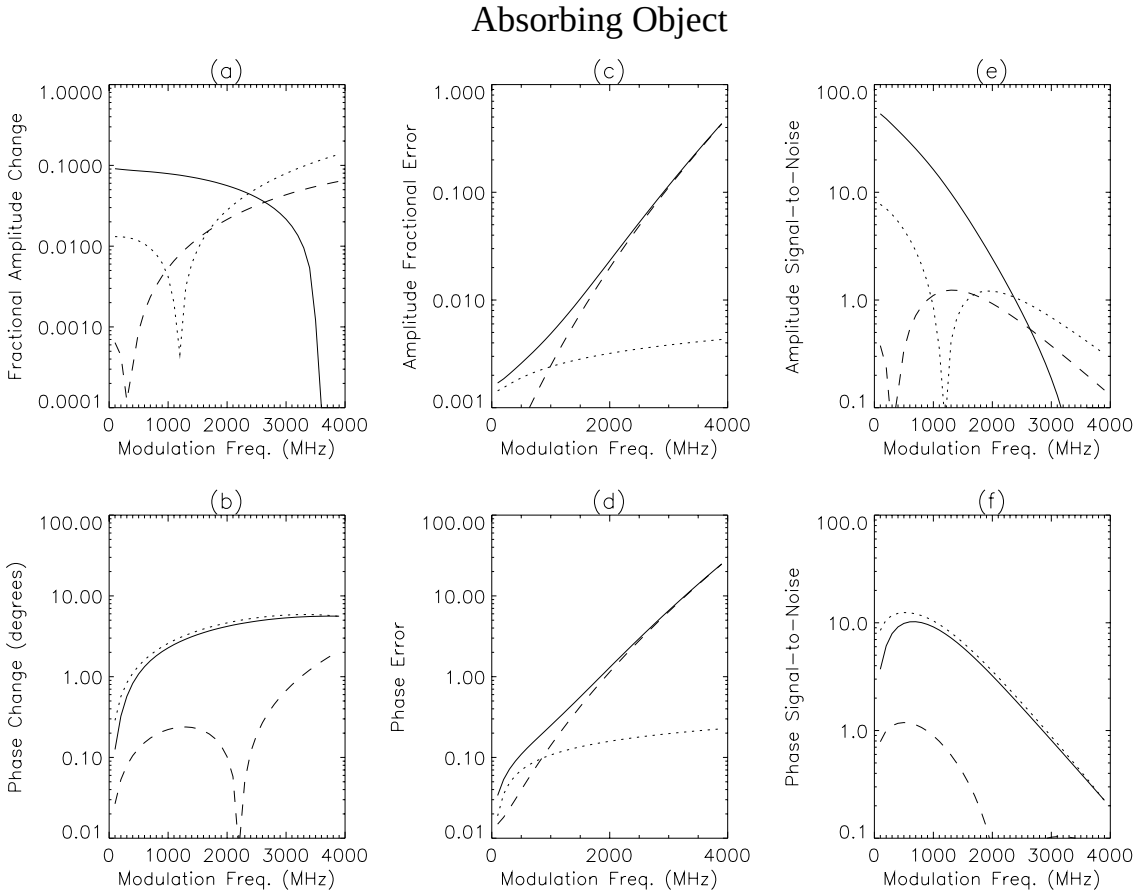

Figure 3.12: The contribution of the monopole (solid line), dipole (dotted line), and quadrupole (dashed line) moments of the scattered wave to the amplitude (a) and phase (b) of the total wave is plotted versus the modulation frequency of the source. The source and detector are separated by 6.0 cm with a 1.0 cm diameter absorbing object centered between them. The optical properties of the object are given in fig. 3.1. The noise in the amplitude and phase is given in (c) and (d) respectively. The dotted (dashed) line corresponds to the positional (shot) noise. The solid line is the combination of positional and shot noise. The signal to noise ratio for amplitude and phase is given respectively in (e) and (f) for the monopole (solid line), dipole (dotted line), and quadrupole (dashed line) moments.

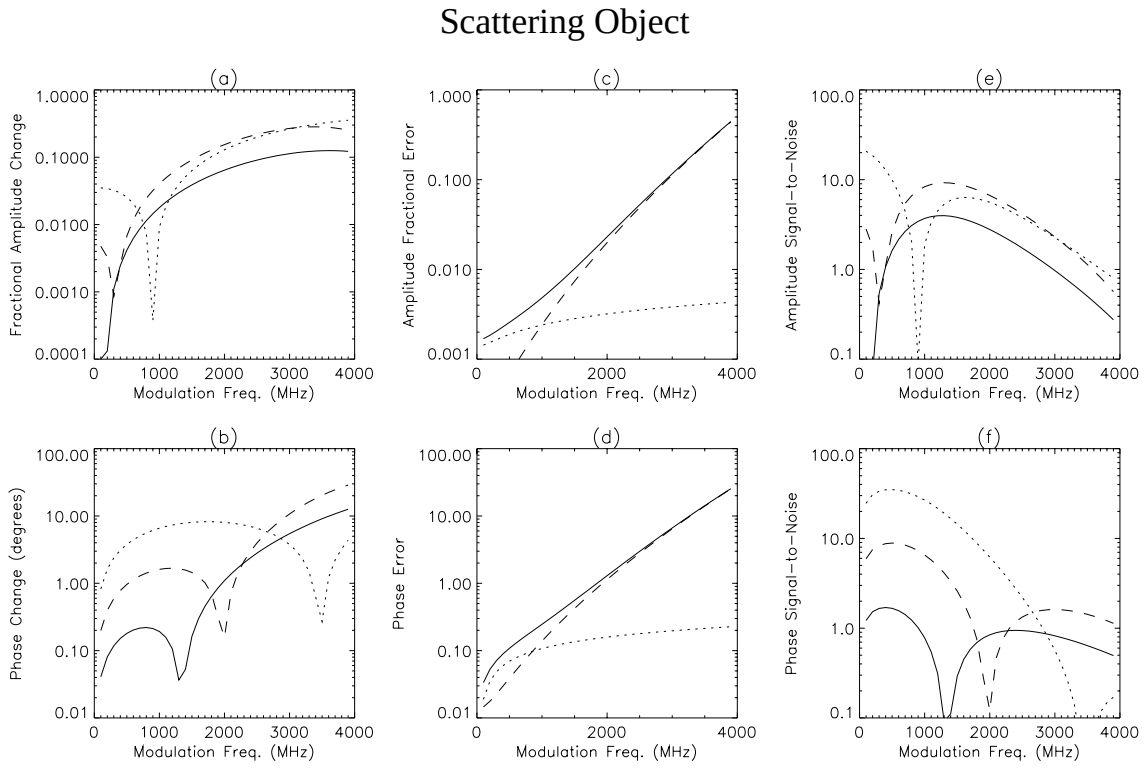

Figure 3.13: The contribution of the monopole (solid line), dipole (dotted line), and quadrupole (dashed line) moments of the scattered wave to the amplitude (a) and phase (b) of the total wave is plotted versus the modulation frequency of the source. The source and detector are separated by 6.0 cm with a 1.0 cm diameter scattering object centered between them. The optical properties of the object are given in fig. 3.1. The noise in the amplitude and phase is given in (c) and (d) respectively. The dotted (dashed) line corresponds to the positional (shot) noise. The solid line is the combination of positional and shot noise. The signal to noise ratio for amplitude and phase is given respectively in (e) and (f) for the monopole (solid line), dipole (dotted line), and quadrupole (dashed line) moments..

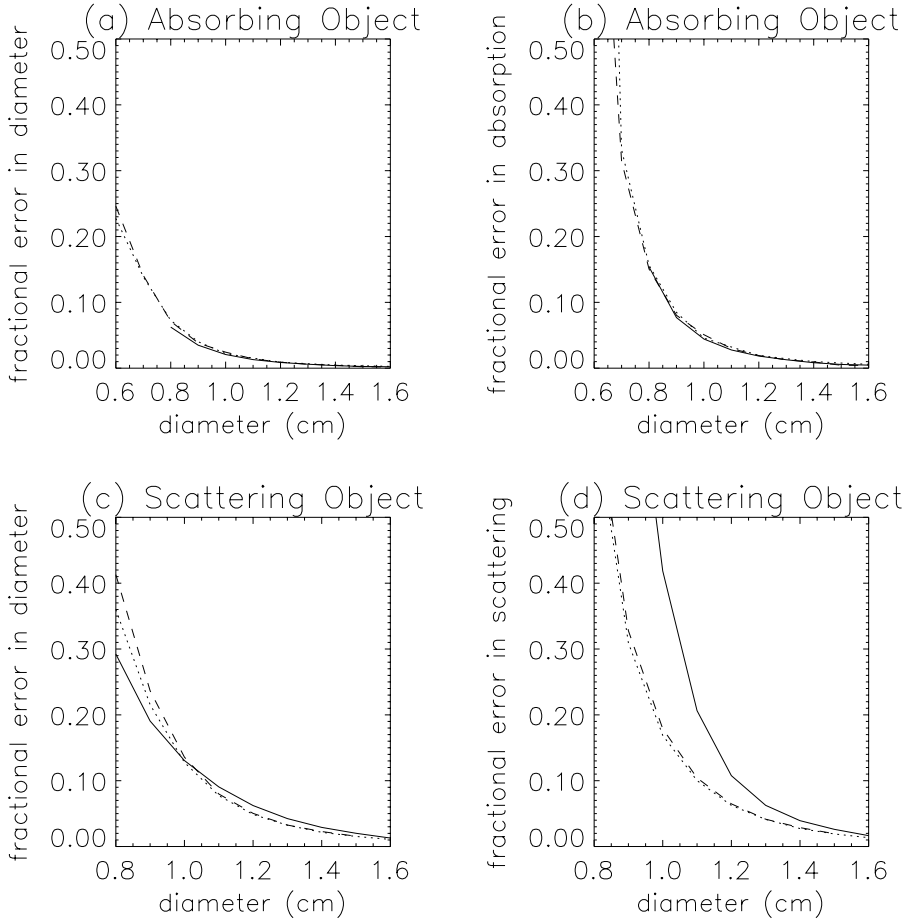

Figure 3.14: The fractional uncertainty in the diameter and absorption coefficient of an absorbing object are given in (a) and (b) respectively versus the diameter of the object. In (c) and (d) the fractional uncertainties are given for a scattering object. Results are given for three different source detector configurations. In all configurations the source was held fixed closest to the object at x=0 and the detector was scanned from x=-2.0 to 2.0 cm in steps of 0.2 cm. The solid lines corresponds to a modulation frequency of 200 MHz with 10 measurements made at each position. The dotted line results from the modulation frequency scanned from 0 to 1000 MHz in steps of 200 MHz with 2 measurements at each position. Finally, the dashed lines corresponds to 1 measurement at each position with the frequency scanned from 0 to 1000 MHz in steps of 100 MHz. Note that the spectral measurements improve the characterization of the scatttering coefficient of the scattering object but do not enhance the characterization of the absorbing object.

3.5.4 Measurements at Multiple Optical Wavelengths

It is reasonable to expect that measurements at multiple optical wavelengths will improve our ability to characterize optical inhomogeneities. I will show that this additional information does not improve our ability to characterize the size and optical properties of inhomogeneities.

Consider two sets of measurements made on the same sample: one at optical wavelength λ_1 and the other at optical wavelength λ_2. For each set we can independently characterize the size and absorption coefficient of the object. Assuming that a common chromophore is the dominant absorber at the two optical wavelengths, then the size of the characterized absorber should be the same for each set. Thus, instead of having four unknowns ($a(\lambda_1)$, $\mu_a(\lambda_1)$, $a(\lambda_2)$, and $\mu_a(\lambda_2)$), we only have three, and three parameters can be characterized more accurately than four.

This argument may sound reasonable, but we have to be careful. It is true that the uncertainties in the three parameters will be smaller than the uncertainties determined for the four parameters when the two data sets are characterized independently. However, will the uncertainties be any smaller than if all measurements were made at a single wavelength? Let's say that each data set has N measurements. In the first case we are using N measurements to get $a(\lambda_1)$ and $\mu_a(\lambda_1)$ and N measurements to get $a(\lambda_2)$ and $\mu_a(\lambda_2)$. In the second case we are using $2N$ measurements to determine a, $\mu_a(\lambda_1)$, and $\mu_a(\lambda_2)$. We would do better to use $2N$ measurements to find just two parameters, a and $\mu_a(\lambda_1)$.

What if we knew the absorption spectrum of the dominant chromophore at λ_1 and λ_2? In this case there would only be two unknowns since $\mu_a(\lambda_1)$ and $\mu_a(\lambda_2)$ would have a known proportionality C. This might lead to improved characterization. To see if this is possible we must consider the extended minima (or valleys) of the chi-squared surfaces for the different data sets. For a two dimensional chi-square function, there is a valley which indicates the relation between systematic deviations in the two fitting parameters. The valley for fitting $a(\lambda_1)$ and $\mu_a(\lambda_1)$ may look like curve 1 in fig. 3.15. This curve tells us what the deviation in a will be if we know the deviation

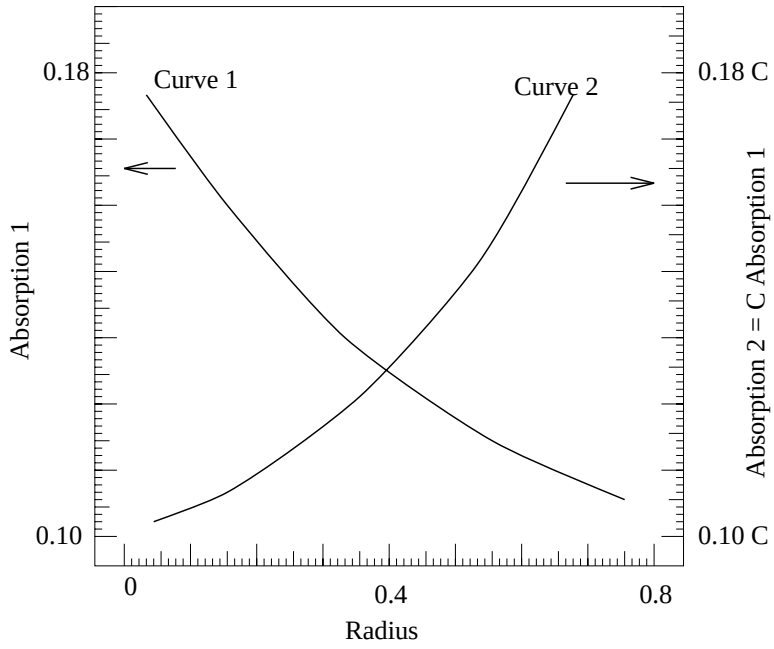

Figure 3.15: Possible chi-squared valleys for a two parameter fit for the object radius and absorption coefficient at two different optical wavelengths.

in μ_a and vice versa. For repeated measurements of the λ_1 data set, the determined a and μ_a values will always appear on curve 1. For λ_2 the valley may look like curve 2 in fig. 3.15. Curve 1 and curve 2 intersect at the correct values for the object parameters. If we fit both data sets simultaneously with the constraint that $a(\lambda_2) = a(\lambda_1)$ and $\mu_a(\lambda_2) = C\mu_a(\lambda_1)$ then the fitting parameters will be drawn towards the intersection point of the two curves, decreasing the uncertainty. If the valleys nearly overlap, then the fitting parameters will not be strongly drawn towards the intersection point. Improved characterization is possible only if the different curves have significantly different slopes near the intersection point.

Valleys for three spherical objects with different absorption coefficients but the same radius are shown in fig. 3.16. The dotted, dashed, and dot-dashed lines were derived from simulations for 5 mm diameter absorbers with absorption coefficients of 0.15, 0.45, and 0.75 cm^{-1}, respectively, relative to the background coefficient of 0.05 cm^{-1}. The other system parameters are indicated in fig. 3.1. These valleys

nearly overlap and therefore we cannot use multiple optical wavelengths to improve object characterization. Even if the curves were more perpendicular, uncertainties associated with the dominant chromophore assumption would reduce any gains in object characterization.

3.6 Summary

The interaction between DPDW's and optical inhomogeneities provides a staightforward way of detecting and localizing inhomogeneities and a means for characterizing the size and optical properties of the inhomogeneity. If no noise were present in the measurements then our ability to characterize these objects would only be limited by the validity of the model used for the analysis. Here, I have used an exact analytic model for the scattering of DPDW's from spherical inhomogeneities which is based on the diffusion approximation to the photon transport equation. This model is valid on length scales larger than the photon random walk step, $1/\mu_s'$, which is around 1 mm for tissue. Unfortunately noise is always present, and, as we have seen, it diminishes our ability to characterize inhomogeneities.

Detecting and locating inhomogeneities is possible if the perturbation of the incident DPDW, the signal (see eq. (3.8)), is greater than the noise threshold. The results presented here demonstrated that 3 mm diameter objects are detectable for realistic parameters. For small absorbing objects the signal is dominated by the monopole moment, while for small scattering objects the signal is dominated by the dipole and quadrupole moments. For transmission measurements, the strongest signal occurs when the object is directly between the source and detector and therefore a detectable object is easily located. Changing the modulation frequency does not greatly change the detectability of absorbing or scattering objects except at high frequencies where the signal is obscured by shot-noise (see figs. 3.4, 3.6, 3.12, and 3.13). The detectability of objects with different optical properties embedded in the same system as described in fig. 3.1 can be determined from the leading order form of the moments of

the scattered DPDW (see eqs. (3.2-3.4)). For instance, the leading order signal from a small absorbing object is proportional to $a^3\delta\mu_a$. This product, $a^3\delta\mu_a$, indicates how much larger a less absorbing object must be or how much smaller a more absorbing object can be in order for it to still be detectable. In particular, the product shows that the size of a detectable object scales as $\delta\mu_a^{-1/3}$. For example, given that an object with $\delta\mu_a$=0.1 cm^{-1} is detectable if $a > 0.3$ cm, then an object with $\delta\mu_a = 0.05$ cm^{-1} is detectable if $a > 0.38$ mm.

Characterizing the size and optical properties of an object is not as straightforward because an indirect method is required, e.g. chi-squared fitting, to determine the parameters from measurements of the distorted DPDW. Furthermore, it is necessary for more than one moment of the scattered DPDW to perturb the signal by a detectable amount in order to distinguish the contributions from the object's size and optical properties. To determine the size and either the absorption or scattering coefficient of an object, it is necessary for two moments to be detectable (i.e. two unknowns and two equations). Likewise, to accurately determine three parameters, it is necessary for at least three moments to be detectable. Because of these additional requirements, inhomogeneities cannot be accurately characterized unless they are 1 cm or larger in diameter for realistic parameters.

I have demonstrated that the measurement geometry can be optimized in order to characterize smaller objects. The only useful measurements are those for which the perturbation is detectable. Therefore, for transmission through a slab geometry it is best to make measurements with the source closest to the object and the detector scanned near the point of closest approach to the object or vice-versa. I have also demonstrated that 0 MHz is the optimal frequency for detecting and characterizing absorbing objects. Scattering objects are best detected and characterized with modulation frequencies near 500 MHz. Characterization of scattering objects is further optimized using measurements at several modulation frequencies.

Still smaller objects can be characterized if there is a priori knowledge of the size or optical properties of the object. For example, knowledge of the structural properties

of the system obtained from a CAT scan or MRI affords an accurate determination of the optical properties of tumors smaller than 1 cm. By reducing the number of unknowns, accurate tumor characterization becomes feasible with the detection of fewer multipole moments. If we know the size of an absorbing or scattering object, then the optical contrast can be determined as long as the contribution from a single moment is detectable. Likewise if the optical contrast is known and the size is sought. Thus, with prior knowledge it is possible to accurately characterize detectable objects, i.e. objects on the order of 3 mm in diameter. Any uncertainty in the priorly known quantity will result in a systematic error in the determined quantity. For example, if the size of the object is measured using MRI to be 5 mm and it is actually 4 mm, then the reconstructed absorption coefficient will be systematically reduced by 50%. The systematic deviation in the absorption (scattering) coefficient of an absorbing (scattering) object due to an incorrect previous determination of the size is described by the universal curve presented in fig. 3.16. The solid line derives from the $a^3\delta\mu_a$ ($a^3\delta\mu_s'$) dependence of the dominate contribution to the scattered wave from an absorbing (scattering) object and indicates that an overestimation of the size results in an underestimation of the optical parameter and vice versa. The dotted, dashed, and dot-dashed lines were derived from simulations for 5 mm diameter absorbers with absorption coefficients of 0.15, 0.45, and 0.75 cm^{-1}, respectively, relative to the background coefficient of 0.05 cm^{-1}. The observed deviation from the universal curve (solid line) arises from the increased importance of higher order multipole moments. This deviation is small and thus the universal curve serves as a good rule of thumb. Note that this result is valid for objects of general shape by replacing a^3 with the volume of the object.

The limits discussed here for detecting and characterizing optical inhomogeneities with diffuse photon density waves are based on ideal systems where the noise is governed by shot-noise and positional errors. The results should thus be viewed as a best case scenario. In the clinical environment, other sources of noise are expected to exist that will further complicate the accurate characterization of optical inhomogeneities. For instance, the intrinsic fluctuations of a biological sample about its average

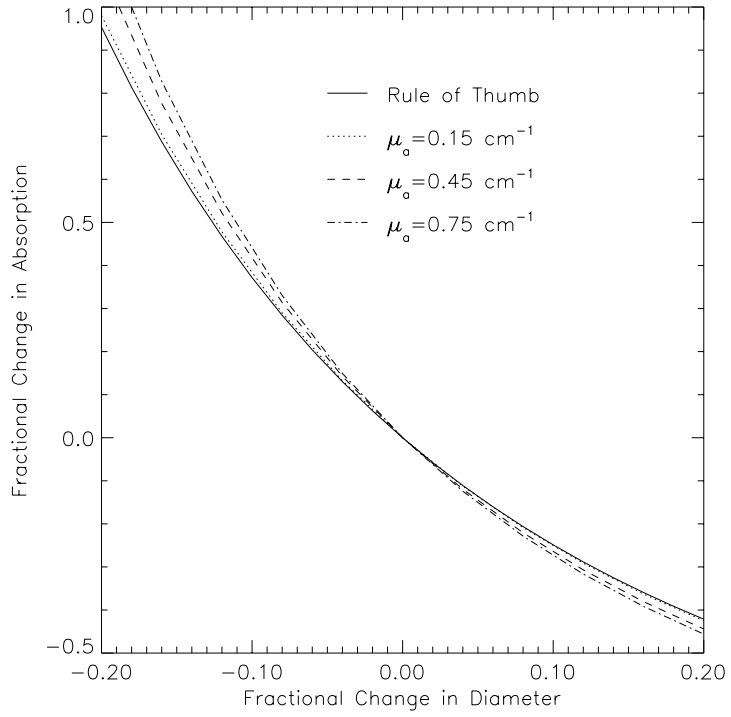

Figure 3.16: The fractional deviation in the optical parameter versus the fractional deviation in the diameter is graphed. The optical paremeter represents either the absorption coefficient or scattering coefficient.

background value causes amplitude and phase shifts. If the intrinsic heterogeneity is not considered in imaging algorithms, then the corresponding signal fluctuations are essentially noise. Quantification of the intrinsic heterogeneity of different biological samples is necessary to determine if this type of noise is significant. Another source of systematic noise is the discrepancy between diffusion models and experiment. A discrepancy between models and experiment of 1% amplitude and a few degrees phase is not uncommon, especially at higher modulation frequencies. Further investigation is required to determine the effect of this systematic noise on optical imaging.